Eye Opening Rapidly Induces Synaptic Potentiation and Refinement

Wei Lu and Martha Constantine-Paton*
Department of Biology
Department of Brain and Cognitive Science
McGovern Institute for Brain Research
Massachusetts Institute of Technology
Cambridge, Massachusetts 02139

Summary

NMDA receptor (NMDAR)-mediated increases in AMPA receptor (AMPAR) currents are associated with long-term synaptic potentiation (LTP). Here, we provide evidence that similar changes occur in response to normal increases in sensory stimulation during development. Experiments discriminated between eye opening-induced and age-dependent changes in synaptic currents. At 6 hr after eye opening (AEO), a transient population of currents mediated by NR2B-rich NMDARs increase significantly, and silent synapses peak. Sustained increases in evoked and miniature AMPAR currents occur at 12 hr AEO. Significant changes in AMPAR:NMDAR evoked current ratios, contacts per axon, and inputs per cell are present at 24 hr AEO. The AMPAR current changes are those seen in vitro during NMDAR-dependent LTP. Here, they are a consequence of eye opening and are associated with a new wave of synaptic refinement. These data also suggest that new NR2B-rich NMDAR currents precede and may initiate this developmental synaptic potentiation and functional tuning.

Introduction

Considerable evidence links NMDA receptor (NMDAR) function to activity-dependent synapse development in vivo (Cline et al., 1987; Bear et al., 1990; Simon et al., 1992; Li et al., 1994; Wu et al., 1996; Zhang et al., 2000). These studies suggest that NMDAR-dependent long-term synaptic potentiation (LTP), in which NMDAR currents initiate AMPA receptor (AMPAR) activation in the postsynaptic membrane (Malinow and Malenka, 2002), is an essential part of the developmental consolidation and refinement of synapses (Constantine-Paton and Cline, 1998). However, only a few studies have attempted to link normal in vivo developmental changes in input activity to the rapid AMPAR current and synapse number increases that are predicted by the NMDAR-dependent LTP model (Durand et al., 1996; Wu et al., 1996; Chen and Regehr, 2000; Hohnke et al., 2000).

In a previous investigation from our laboratory, eyes of rat pups were glued shut before eye opening (EO) and then opened on P11, P13, and P16 (Yoshii et al., 2003). Compared to littermates whose eyes were not opened, in these animals large increases in the NMDAR scaffolding protein PSD-95 were invariably present in central visual neuron dendrites within 6 hr of this con-

*Correspondence: mcpaton@mit.edu

trolled EO. A transmembrane AMPAR-stabilizing molecule of the stargazin family (Schnell et al., 2002; Tomita et al., 2003) was bound to the dendritic PSD-95 and increased proportionately with PSD-95 after eye opening (AEO). However, there were differences in the relative amounts of NMDAR NR2 subunits bound to this dendritic PSD-95 AEO; whereas there was more NR2B bound to PSD-95 before eye opening (BEO), NR2A became the prominent subunit bound to PSD-95 AEO. These changes prompted us to ask whether functional changes in glutamatergic visual synapses were detectable at similarly short latencies. Using the EO paradigm of Yoshii et al. (2003) to induce and synchronize vision-driven changes occurring with natural EO, we studied evoked and spontaneous NMDAR and AMPAR currents at hours and days AEO in rat pups and in age-matched littermates with eyelids that were never opened (ENO). Our results from acute whole-cell slice recordings indicate that a long-lasting potentiation of AMPAR currents is present by 12 hr AEO in vivo. The data support several other investigations that show increased long-lasting potentiation of AMPAR currents following transfection-induced increases in postsynaptic PSD-95 (Beique and Andrade, 2003; Stein et al., 2003; Ehrlich and Malinow, 2004). However, in contrast to the transfection work, our developmental studies indicate that the earliest AMPAR current increases are preceded by and likely dependent upon a transient population of small currents that are mediated selectively by NR2B-rich NMDAR currents that increase rapidly AEO. Also, in the present work, the stereotyped current changes AEO are associated with synaptic refinement: a decrease in the number of inputs to single postsynaptic neurons and an increase in the active sites supported by the inputs that survive.

Results

Recordings were made in the superficial visual layers of the superior colliculus (sSC). Comparisons between glutamate currents in EO and ENO littermates were begun at 6 hr AEO, a time at which EO-induced increases in dendritic PSD-95 plateau (Yoshii et al., 2003). Currents were also studied at progressively longer intervals of 12 and 24 hr and 3 and 7 days AEO. NMDAR current changes were the first to be observed. At the ages studied here, the retinocollicular map shows adult-like organization at the light microscope level, and the corticocollicular projection has begun to arborize profusely in the sSC.

Two Populations of Spontaneous NMDAR Currents at 6 Hr AEO

Spontaneous NMDAR (sNMDAR) currents were studied in the absence of tetrodotoxin (TTX) to minimize masking small events in the baseline noise. Almost all spontaneous currents BEO were relatively large and fast, indicative of the mixture of NR2A- and NR2B-containing receptors that were previously documented in the sSC from P10 to P13 (Shi et al., 2000). However, two distinctly
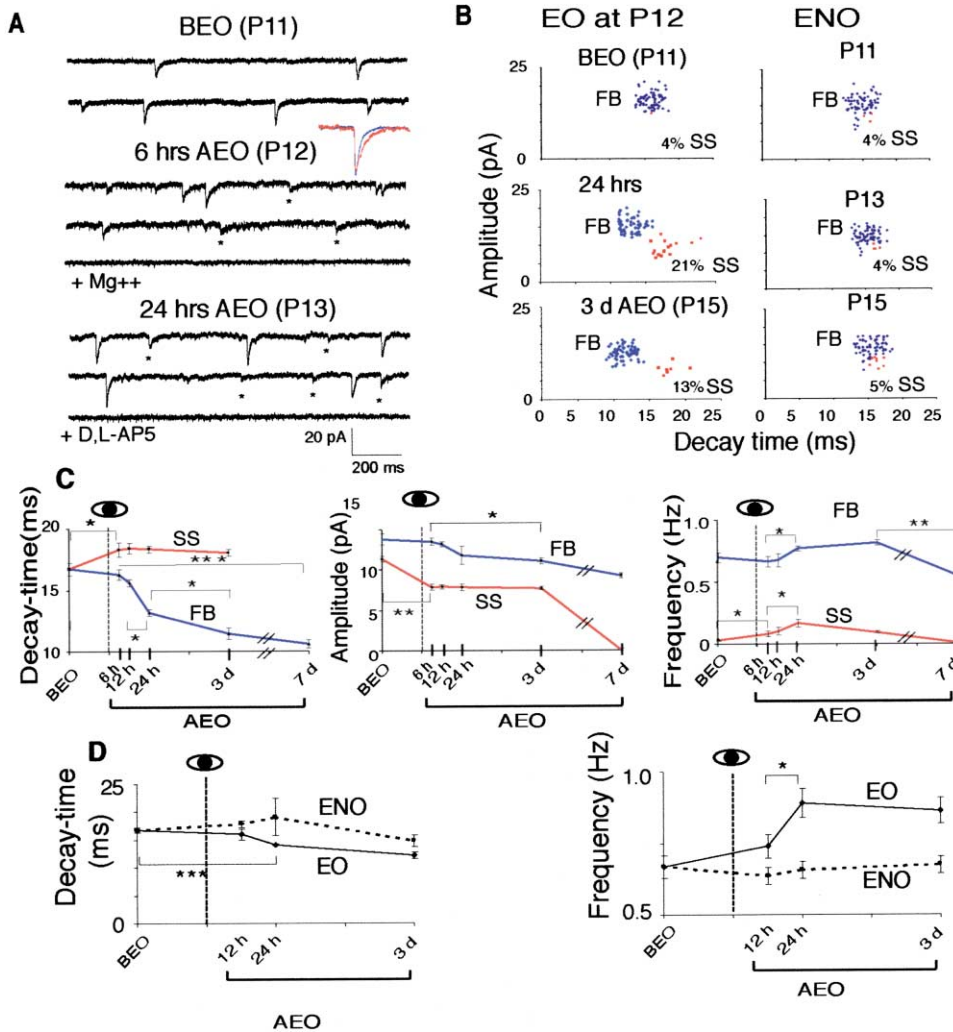
Figure 1. Two Distinct Populations of Spontaneous NMDAR Currents Are Present at 6 Hr AEO

(A) Traces showing spontaneous NMDAR (sNMDAR) currents recorded BEO and at short intervals AEO. A population of slowly decaying and small amplitude currents (SS; asterisks) along with generally faster and bigger (FB) currents are seen at 6 and 12 hr AEO. Both populations are abolished by D,L-AP5 or 4 mM Mg^{2+}. (Inset) Typical scaled superposition of averaged SS and FB sNMDAR currents from a neuron 6 hr AEO show indistinguishable rise times but different decay times. (B) Amplitude versus decay time plots for all sNMDAR currents (n = 75) chosen at random from recordings of individual cells at each time point. The plots distinguish the two types of sNMDAR currents. SS currents (amplitudes < 13 pA and decay times > 15 ms) are in red. All other currents, defined as FB currents (see text), are in blue. Percentages reflect the proportion of total sNMDAR currents represented by SS neurons recorded in all neurons of a particular category. In ENO neurons, SS currents are never distinct from FB currents and remain infrequent. (C) sNMDAR current decay time, amplitude, and frequency at different intervals AEO. SS sNMDAR current decay time and amplitude remained stable until their disappearance between 3 and 7 days AEO. FB sNMDAR currents showed a rapid decrease in decay time between 12 and 24 hr AEO and continued a slow decrease for at least 7 days AEO. Frequencies of FB and SS sNMDAR currents increase between 6 and 24 hr AEO. FB currents decrease by 7 days AEO, while SS current frequency peaks at 24 hr AEO. (D) No changes in frequency or decay time of total sNMDARs were observed in ENO littermates, in contrast to the changes that were observed in frequency and decay time of total sNMDARs in the EO pups. n = at least 7 or 8 neurons for each data point except for P13 ENO, where n = 6. In general, for clarity, in this and all other figures where statistical data is graphed, significance is identified only for the two closest time points. The few exceptions to this represent intervals where it is particularly important to illustrate trends over longer intervals.

different populations of sNMDAR currents were apparent at 6 hr AEO (Figure 1). The most frequent were indistinguishable in decay time, amplitude, and frequency from the currents present in littermates BEO. These currents were generally greater than 13 pA in peak amplitude, with average decay times that decreased rapidly from 16 to 13 ms between 12 and 24 hr AEO (Figure 1C). This population was termed fast and big sNMDAR (FB) currents to distinguish them from the smaller slower

(SS) rigidly defined group, even though a minority of FB currents were either fast with lower amplitudes or big with slow decays. The FB population continued to decrease in decay time, frequency, and amplitude until last assessed at 7 days AEO. This may reflect an overall reduction in NMDAR currents as neuropil matures (Fox et al., 1991; Binns and Salt, 1998).

The second, SS population of sNMDAR currents had both small amplitudes (<13 pA) and slow decay times
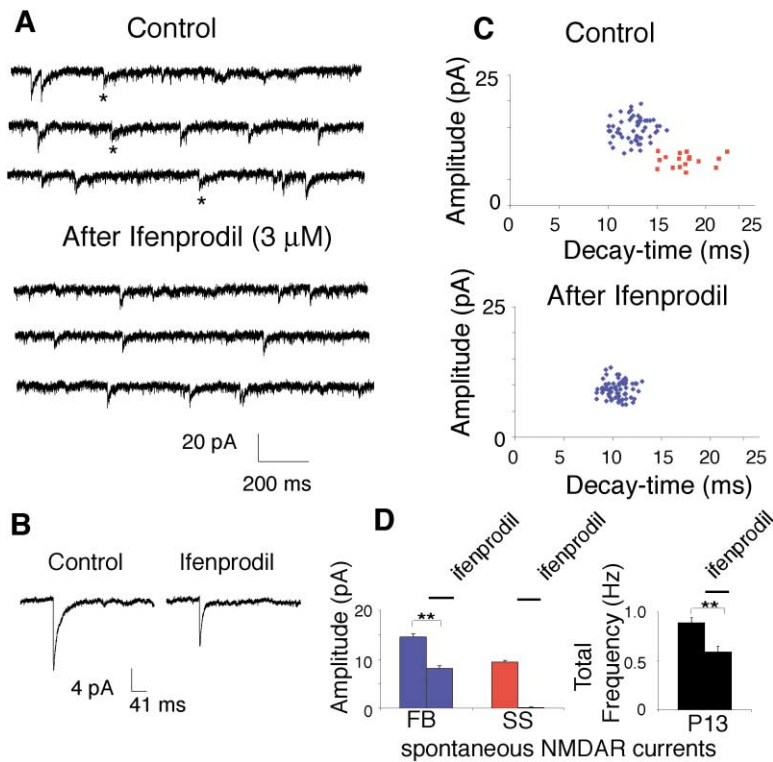
Figure 2. SS sNMDAR Currents Are Mediated by NR2B-Rich Receptors

(A) Recordings of sNMDAR currents 24 hr AEO, before (control) and after the antagonist of NR2B-rich NMDARs (ifenprodil) was perfused into the recording chamber. During ifenprodil application, SS currents disappeared; decay time and amplitude of FB also decreased.

(B) Averaged FB sNMDAR currents before and during ifenprodil application showing the decrease of both amplitude and decay time and indicating a contribution from NR2B-rich receptors.

(C) Amplitude versus decay time plots of sNMDAR currents from a typical neuron show the same effects that were seen in the average currents in (B).

(D) At 24 hr AEO (P13), ifenprodil eliminated SS sNMDARs (left) and produced an overall ~25% frequency decrease in sNMDAR currents. n = 7 or 8 neurons examined for each comparison.

(>15 ms; Figure 1A). SS currents were only 4% of the total number of sNMDAR currents BEO. At 6 hr AEO, the SS population jumped to 11% of the total population, but the average peak amplitude declined, and the average decay time increased significantly (Figure 1B), suggesting that the increased frequency was due to new NMDAR-containing contacts that contained more slow NMDAR currents and fewer receptors. Maintaining these lower amplitudes and longer decay times (9 pA and 18 ms), the SS population peaked at 21% total by 24 hr AEO. At 3 days AEO, they dropped to 13% of the total sNMDAR currents, and at 7 days AEO, SS currents disappeared (Figure 1B, left column, Figure 1C, and Supplemental Figure S1 at http://www.neuron.org/cgi/content/full/43/2/237/DC1). Furthermore, SS currents were present in only ~28% of the recorded neurons at their most prevalent time point (6 hr AEO; Supplemental Figure S1 at http://www.neuron.org/cgi/content/full/43/2/237/DC1). Thus, SS currents may be expressed broadly in sSC neurons but for a short interval in each cell, or they may be transiently present in only a subset of cells. This analysis cannot discriminate these alternatives. Nor can it determine whether changes in corticocollicular inputs, retinocollicular inputs, or all inputs are driving SS currents. Nevertheless, a number of observations suggest a fast conversion of SS into FB currents with time AEO. (1) The rapid appearance and disappearance of a peak in "silent synapses" and the low incidence of such contacts (presented below). (2) Decreased FB amplitudes and increased FB frequencies at 24 hr AEO, when SS current frequencies peak. (3) FB currents that appear to be intermediate between the rigidly defined SS currents and currents that have both large amplitudes and short decay times. (4) As will be seen in Figure 2, some of the

receptors mediating FB currents contain NR2B subunits, while SS currents are mediated by NMDARs that *only* contain the NR2B subunit.

Scaled averages of FB and SS sNMDAR current types were compared (Figure 1A, inset) and revealed nearly coincident rise times, suggesting that the prolongation of SS currents is not due to a more distal dendritic position of the contacts from which they arise. However, this overlap in rise time does not indicate that FB and SS currents are driven by the same projection, because the rough dendritic segregation of cortical and retinal inputs in the mature sSC is unlikely to be established at this age.

A small number (4%–5%) of sNMDAR currents that met the size and decay time criteria of SS currents were observed in neurons from ENO pups (Figure 1B, right column). However, these were never distinguishable as a distinct group in amplitude versus decay time scatter plots from individual neurons. Also, the numbers of SS currents in ENO pups did not change with age. Figures 1D and 1E compare sNMDAR current data averaged at each time point for EO and for ENO pups. The averaging process minimizes decay time changes of FB sNMDARs in the EO group and also obscures the fact that the low frequency of sNMDAR currents in the ENO group is due to the absence of SS sNMDARs.

NMDAR currents with long decay times frequently show a high sensitivity to low concentrations of the atypical NMDAR antagonist ifenprodil, which specifically blocks NR2B-rich receptors (Williams et al., 1993). We examined the subunit composition of the sNMDAR currents using ifenprodil at 24 hr AEO. Ifenprodil reduced the decay time of sNMDAR currents, decreased the amplitude of the average sNMDAR current, and also
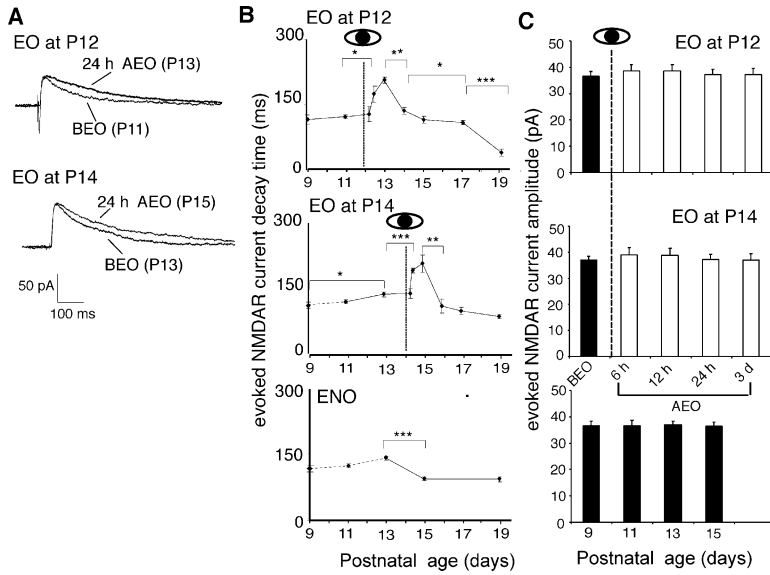
Figure 3. Evoked NMDAR Current Decay Times Increase Transiently between 12 Hr and 48 Hr AEO; Amplitude Remains Constant

(A) Average traces showing increases in evoked NMDAR current decay time at 12 hr and 24 hr AEO when EO occurred at P12 or at P14 AEO.

(B) Quantification of average evoked NMDAR current decay time relative to EO at P12, at P14, and in ENO littermates. The transient increase in decay times peaks at 24 hr AEO, coinciding with the peak frequency in SS sNMDARs. Pups with ENO showed a significant increase in evoked NMDAR current decay time between P9 and P13 (see text). Dotted lines = BEO data in more than one graph. In ENO pups, the increase was followed by a significant decrease between P12 and P13. n = 7 to 12 neurons for all data points except P14 EO, 24 hr AEO, where n = 6 neurons.

(C) Evoked NMDAR current amplitude measured at stimulus strengths midway between threshold and maximal do not change over the same intervals.

decreased sNMDAR frequency (Figures 2A and 2B). Amplitude versus decay time plots for individual sNMDAR currents from single neurons before and after ifenprodil application revealed the reason for this change (Figure 2C). During ifenprodil perfusion, the SS population is absent, and the points representing FB currents cluster in a region of lower amplitude and faster decay time, suggesting that FB currents are not mediated by a homogeneous population of NMDARs but rather that NMDARs enriched in NR2B are contributing some increase in amplitude and some increase in decay time to individual FB events (Figure 2C, lower). Changes are summarized in Figure 2D.

The findings imply that, shortly AEO, some NR2B-rich receptors are still present at the presumably older postsynaptic densities (PSDs) that are responsible for the FB responses, and the first current changes observed after EO are mediated entirely by NR2B-rich NMDARs. NR2B-rich receptors are frequent in newly innervated neuropil (Wu et al., 1996; Shi et al., 1997, 2000) and have been suggested to be the receptors responsible for the initial genesis of glutamate synapses (Tovar and Westbrook, 1999). Thus, the rapid appearance of SS sNMDARs suggests that EO rapidly initiates a new wave of glutamate synaptogenesis.

Transient Increases in Evoked NMDAR Currents Beginning 12 Hr AEO
All evoked currents are likely to incorporate both retinal and collicular inputs, as they were elicited by stimulating electrodes placed in the stratum opticum, where both retinal and cortical afferents are intermixed. NMDAR evoked currents were studied from P9 to P19 and in pups with their eyes opened on P12 (before normal EO) and on P14 (after normal EO). NMDAR evoked current amplitude, measured at the midpoint between the minimal and maximal evoked NMDAR currents, did not change. However, large significant increases in evoked NMDAR current decay times began at 12 hr AEO, peaked at 24 hr AEO, and were gone by 48 hr AEO regardless

of whether EO occurred at P12 or P14. By P19, evoked NMDAR current decay times dropped to intervals shorter than those measured BEO, regardless of whether the eyes had been opened at P12 or at P14 (Figure 3B). The dominant factor producing these large and transient NMDAR evoked current decay times is likely to be currents mediated by the SS NMDAR currents shown in Figure 1. The time course of appearance and disappearance of these long-decay time small currents corresponds closely to the evoked current decay time increase. When studied at +40 mV, all contacts that mediate SS sNMDAR currents would be activated and would contribute their slow decay times to the evoked NMDAR decay time. It is also significant that the NR2A-rich NMDARs bound to dendritic PSD-95 at 6 hr AEO (Yoshii et al., 2003) may be inserting into preexisting synapses during this interval (see the FB currents in Figure 1C), but the expected NR2A-mediated decrease in the NMDAR response (Monyer et al., 1994; Flint et al., 1997) is masked in the NMDAR evoked currents.

In pups with their eyes closed between P9 and P13, a slow increase in evoked NMDAR current decay times was also observed (Figure 3B, two lower graphs). This is consistent with earlier observations that even BEO a slow increase in PSD-95 and NR2A-rich receptors at the center of the synapse is accompanied by previously subsynaptic NR2B-rich receptors localizing to perisynaptic membrane, where they dominate the decay time of evoked NMDAR currents (Townsend et al., 2003). The large transient increases in NMDAR current decay times were never seen in recordings from ENO littermates (Figure 3B, bottom graph). Rather, in these animals, between P13 and 15, neurons showed a decrease in evoked NMDAR current decay time, suggesting continuation of the slow addition of NR2A-rich NMDARs at synapses and a relative decrease in perisynaptic NR2B-rich receptors.

Silent Synapses Peak at 6 Hr AEO
The possibility that SS sNMDAR currents represent an early stage of synaptogenesis motivated a study of silent
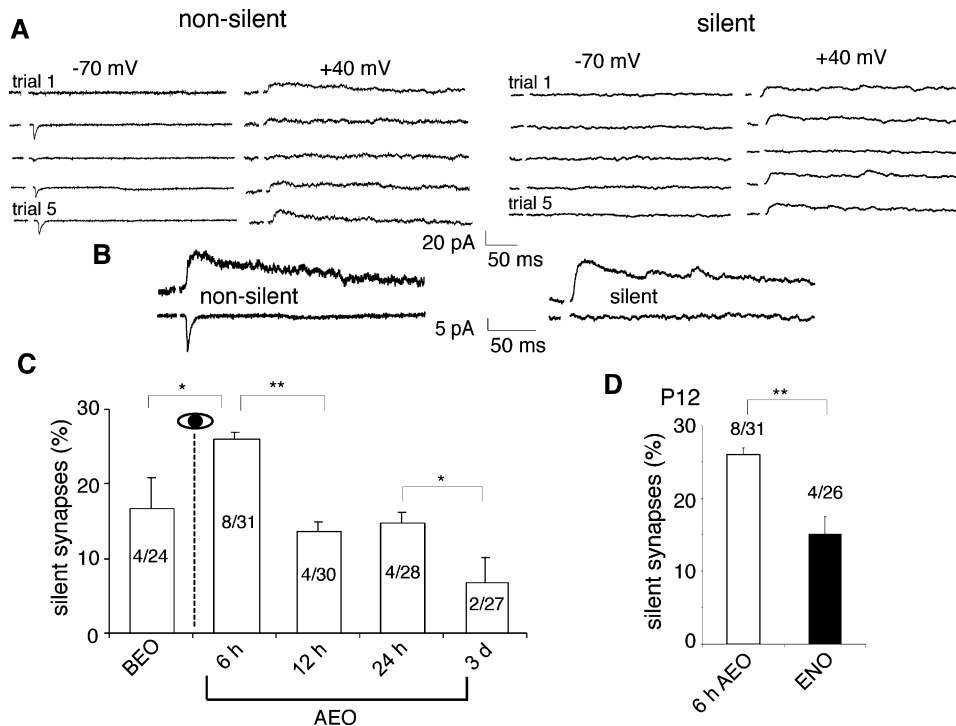
Figure 4. Silent Synapses Show a Transient Increase at 6 Hr AEO

(A) Sample recordings show five trials of minimal evoked EPSCs at a nonsilent and at a silent synapse with the cells held at −70 mV and at +40 mV.

(B) Averages of the recordings in (A).

(C) Histograms of the percentage of neurons with silent synapses as determined by the minimal stimulation paradigm. Each data point is the average of the average of all neurons from the same litter to give a mean silent/nonsilent synapse percentage across litters for each time point and treatment. Data are from three litters for BEO and 3 days AEO and four litters for the remaining points.

(D) The percentage of silent synapses at 6 hr AEO is significantly greater than the percentage of silent synapses in age-matched littermates with ENO at the same 6 hr time point. Neuron numbers for each time point are above each histogram bar.

synapses in the sSC neuropil AEO. Silent synapses show an NMDAR current when a minimal stimulus is applied to a neuron held at +40 mV but lack AMPAR current when the holding potential is ∼−70 mV. Such "NMDAR only" synapses are frequently found in young neuropil in which NMDAR currents have not yet been sufficiently active to drive AMPARs into the postsynaptic membrane (Isaac et al., 1997; Durand et al., 1996). If EO initiated a new period of synaptogenesis, then more silent synapses should be present AEO. Neurons from pups BEO and at 6 hr, 12 hr, 24 hr, and 3 days AEO were examined for silent synapses (Figure 4A). Three to four litters were used at each interval, and the proportion of silent synapses from each litter was averaged to obtain the graph shown in Figure 4C. Cells with silent synapses were scarce. However, this proportion peaked at 6 hr after EO.

Decay times of evoked NMDAR currents from silent synapses at 6 hr AEO (n = 8 neurons) were compared to evoked NMDAR currents from ten randomly selected, nonsilent synapses that were recorded at 6 hr AEO. The average outward NMDAR current at the silent synapses was significantly longer than the average at nonsilent synapses (188.0 ± 3.4 ms versus 156.3 ± 4.8 ms; $p < 0.01$), supporting the hypothesis that many of the SS NR2B-rich NMDAR currents at 6 hr AEO represent founding receptors at nascent synaptic contacts.

Miniature AMPAR Current Changes Are Present at 12 Hr AEO

Miniature AMPAR currents were examined BEO and AEO to test for increases in miniature AMPAR current amplitude diagnostic of AMPAR addition to PSDs (Oliet et al., 1996) and increased AMPAR current frequency indicative of new AMPAR-containing contacts. Miniature AMPAR current amplitude and frequency increases were first detected at 12 hr AEO (Figures 5A and 5B). Some increases with age in miniature AMPAR current amplitude and frequency were detected in animals with ENO (Figures 5C and 5E), but these increases were small and slow compared to the rapid changes in the EO group (Figures 5C and 5D; Sign test; amplitude, $p < 0.05$; frequency, $p < 0.01$). Thus, EO-associated increases in AMPAR currents lag EO-associated increases in NMDAR currents and the peak in silent synapses by up to 6 hr.

Increases in evoked AMPAR currents were also detected at 12 hr AEO as increases in the maximal evoked AMPAR current amplitudes (Figure 6A). However, increases in AMPAR:NMDAR evoked current amplitude and density ratios were not detected until 24 hr AEO (Figure 6B). In addition, non-NMDAR/NMDAR peak current amplitude ratios had the same long latency irrespective of whether EO occurred at P12 or P14, sug-

A average miniature AMPAR currents

BEO

12 h AEO

4 pA
10 ms

B miniature AMPAR currents

BEO

AEO {
6 h
12 h
24 h
3 d
}

20 pA
10 s
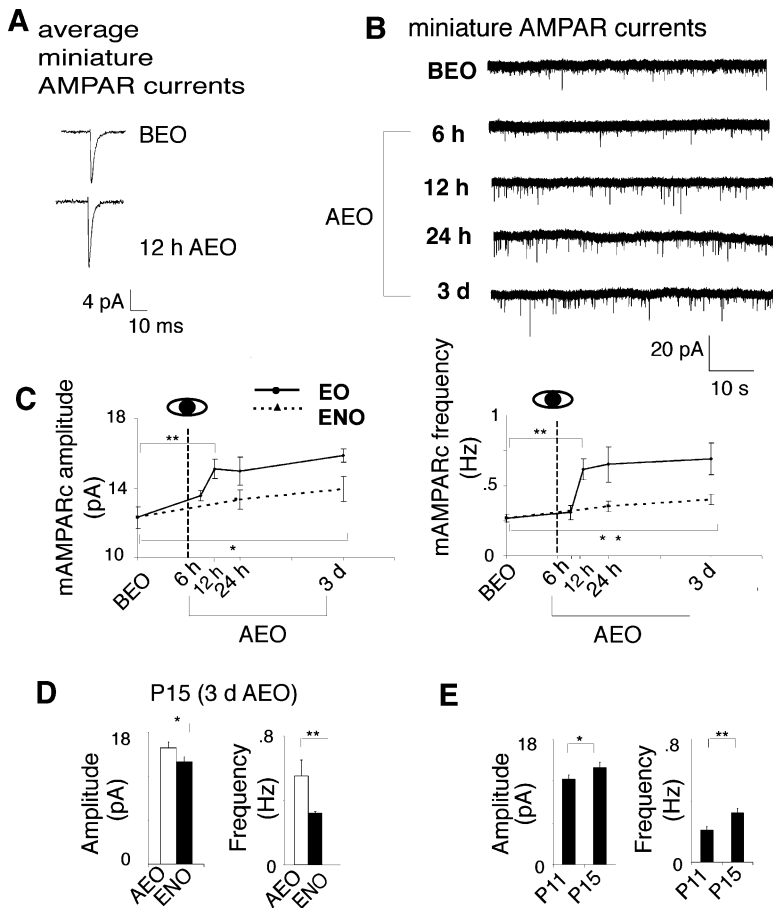
C

D P15 (3 d AEO)

E

Figure 5. Potentiation of Pure Miniature AMPAR Current Amplitude and Frequency at 12 Hr AEO

(A) Typical average miniature AMPAR current (mAMPARc) traces BEO and at 12 hr AEO on P12.

(B) Representative recordings of mAMPARcs showing the frequency increase between 6 hr and 3 days AEO.

(C) Quantitative changes in mAMPARc amplitude (left) and frequency (right) relative to the time AEO. The dotted lines indicate data from age-matched littermates with ENO. n = at least 7 and up to 9 neurons for each data point.

(D) Histograms comparing mAMPARc amplitude (left) and frequency (right) in age-matched littermates with EO for 3 days (white bar) and ENO (black bar). Significance was tested using the nonparametric paired sample Sign test, because the variance from ENO animals was smaller than the variance from EO littermates. n = 7 neurons for each point.

(E) Histograms comparing the mAMPARc amplitude (left) and frequency (right) in animals with ENO between P11 and P15 show significant increases only at the longest interval (3 days). n = 7 neurons for each data point.

gesting that the lag was not due to a developmental limitation on non-NMDAR subunit availability (see Supplemental Figure S3 at http://www.neuron.org/cgi/content/full/43/2/237/DC1).

Cells from ENO littermates also showed a significant increase in AMPAR:NMDAR evoked current ratios from BEO to 24 hr AEO. However, these differences occurred in smaller increments and were smaller in absolute size (Figure 6B and 6C; Sign test; p < 0.01).

Presynaptic Release AEO

The paired pulse ratio (PPR) of evoked AMPAR currents BEO and at each of the AEO time points was examined (see Supplemental Figure S2 at http://www.neuron.org/cgi/content/full/43/2/237/DC1). No changes in the PPR were evident over any of the intervals, suggesting that the probability of transmitter release at the synapses that were studied did not change over the time period that was studied. The changes documented above are likely to be post- and not presynaptic.

Evidence of Structural Rewiring of Local sSC Circuits as a Rapid Response to EO

Increases in Active Sites per Input AEO

The silent synapse data suggest that some new NMDAR/AMPAR synapses are being formed and maintained from the onset of EO until at least 3 days AEO. Such an addition of new contacts is believed to be a long-term effect of NMDAR-dependent LTP called long long-term potentiation (Bolshakov et al., 1997; Toni et al., 1999).

We asked if the new synapses in the sSC reflected a net increase in active sites per axon when compared with BEO inputs—an outcome expected if effective inputs are being reinforced by acquisition of release sites AEO. Relative changes in the minimal number of active release sites per axon (input) were estimated by assuming a release probability of 1, obtaining an average minimal AMPAR evoked current (Figure 7A), and dividing this average by the average of miniature AMPAR current amplitudes for that neuron. The probability of vesicle release at most release sites is much less than 1, implying that numbers obtained with this method are gross underestimates. Nevertheless, they do show significant and rapid changes. Figure 7B plots the data for neurons recorded BEO and at 12 hr, 24 hr, 3 days, and 7 days AEO and from ENO littermates. The minimal number of active sites per input increased between 12 and 24 hr AEO and between 24 hr and 3 days AEO. An increase in active sites per axon was only detected in ENO animals between 12 hr and 3 days AEO, and the ENO increases were significantly smaller than those seen in age-matched EO pups (Sign test; P13, P15, P17; p < 0.05). Therefore, EO and the subsequent NMDAR and AMPAR current changes that were induced by the event facilitate increases in the number of synapses converging on one postsynaptic cell from single innervating axons.

Synapse Elimination on the Single-Cell Level AEO

Activity patterns can shape local synaptic circuitry only if inputs that are not sufficiently strong or cooperative with other inputs are eliminated. To determine whether

A

max. evoked AMPAR current (pA)

109.44
72.51

BEO (P11)   12 h AEO (P12)

B   EO at P12
□ EO
■ ENO

Evoked AMPAR/ NMDAR Current Ratio

peak amplitude

density

BEO 6 h 12 h 24 h 3 d
AEO

C

P13   P15

Evoked AMPAR / NMDAR Current Ratio

peak amplitude

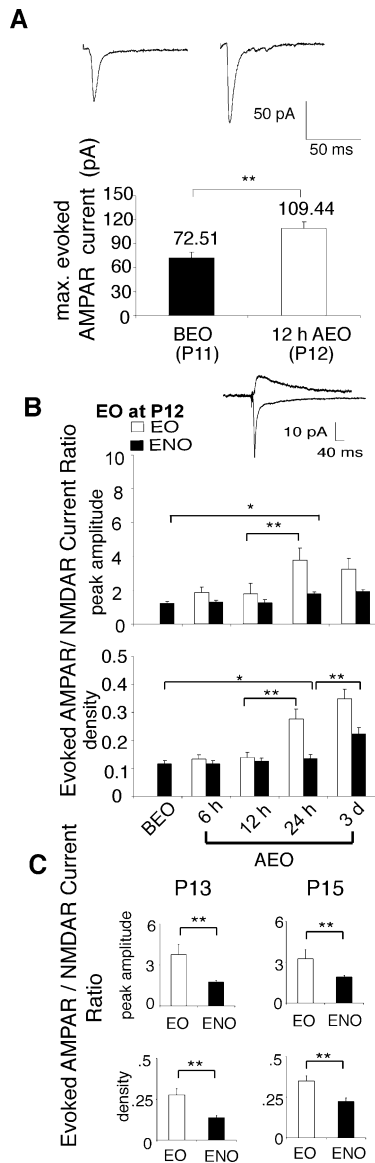EO ENO   EO ENO

density

EO ENO   EO ENO

Figure 6. Potentiation of Evoked AMPAR Current Amplitude at 12 and 24 Hr AEO

(A) Representative average AMPAR evoked current responses to maximal stimulation BEO and 12 hr AEO (top). Quantitation of these increases in amplitude (bottom). n = at least 6 neurons for each bar.
(B) Evoked AMPAR:NMDAR current amplitude ratios AEO at P12 (white bars, top graph) or current density ratios (white bars, bottom graph). Black bars represent data from age-matched ENO littermates. (Inset) Typical AMPAR and NMDAR currents evoked by stimulating intensities approximately halfway between threshold and saturation. n = at least 9 neurons for each bar except for 3 days AEO, when n = 7 neurons. A significant jump in these ratios occurred in EO animals between 12 and 24 hr AEO. In ENO animals, a significant change in AMPAR:NMDAR ratios appeared at longer intervals: BEO to 24 hr AEO and BEO to 3 days AEO.
(C) Comparisons between EO and ENO littermates at P13 and P15 all show highly significant increases in ratios from EO pups relative to the ENO pups.

increases in synapse elimination in the sSC were time-locked to EO, we applied the "method of shoulders" (Purves and Lichtman, 1985). In Mg^{2+}-containing ACSF with $GABA_A Rs$ blocked and a holding potential of -70

mV, non-NMDAR-mediated jumps in synaptic current to successively stronger electrical stimuli were recorded. At each stimulus level, several stimuli were applied to assure that an increase was stable. Each stable jump in response current was scored as a separate input. The method provides a rough estimate of the number of axons in the stimulated bundle that make excitatory contacts on the patched neuron. As neuropil matures, the number of discrete jumps in the amplitudes of the excitatory currents gives a relative measure of changes in the number of different axons terminating onto a post-synaptic neuron over time (Figure 7C). Estimates of inputs in EO and ENO littermates are shown in Figure 7D. At each of the time points that were studied, littermates with EO showed significantly lower numbers of different inputs than their ENO siblings. The most rapid synapse elimination occurred during the first 24 hr AEO (Figure 7E), concurrent with most of the receptor current changes described above.

Discussion

Eyelid opening and the consequent initiation of high-resolution pattern vision are necessary for the final stages of activity-mediated tuning in the developing visual pathway. The many studies of this tuning have provided broad insight into the epigenetic organization of the brain (Singer, 1995). However, despite this large literature, few studies have focused on the immediate cellular and synaptic responses to the EO event itself. EO in rodents occurs over the course of 1–2 days, and synaptic responses are similarly dispersed in time, making them difficult to study. Synchronizing synaptic responses to EO by controlling EO and comparing data between siblings with and without EO has identified the following stereotyped sequence of responses specifically tied to the EO event. Spontaneous NMDAR currents that are mediated by NR2B-rich NMDARs and a transient peak in silent synapses are present by 6 hr. By 12 hr, a significant increase in the amplitude and frequency of miniature AMPAR currents is evident. Simultaneously, evoked NMDAR currents begin a large but transient increase in decay time that is gone by 2 days AEO. By 24 hr, evoked AMPAR:NMDAR current ratios are significantly increased, and a decay time decrease indicating an increase in NR2A-rich NMDARs is seen in FB sNMDAR currents. These current alterations are accompanied by an increase in the number of active sites per input and by a decrease in the number of different axons that innervate each sSC neuron. The former is present during long long-term potentiation in the hippocampus (Bolshakov et al., 1997; Toni et al., 1999), while the latter is associated with activity-dependent synapse elimination during development (Purves and Lichtman, 1985).

This work focused on the superficial, visual layers of the sSC and a limited number of sSC cell types, most likely narrow field vertical cells and some larger piriform neurons (Langer and Lund, 1974). Most sSC neurons receive direct input from the ganglion cells of the contra-lateral retina (Lund, 1972; Drager and Hubel, 1976; Linden and Perry, 1983). At EO, topographic refinement of the retinocollicular map is complete (Simon and O'Leary, 1992), and photoreceptors have begun to drive retinal ganglion cells, even though the eyes are still closed (Bansal et al., 2000; Townsend et al., 2003).
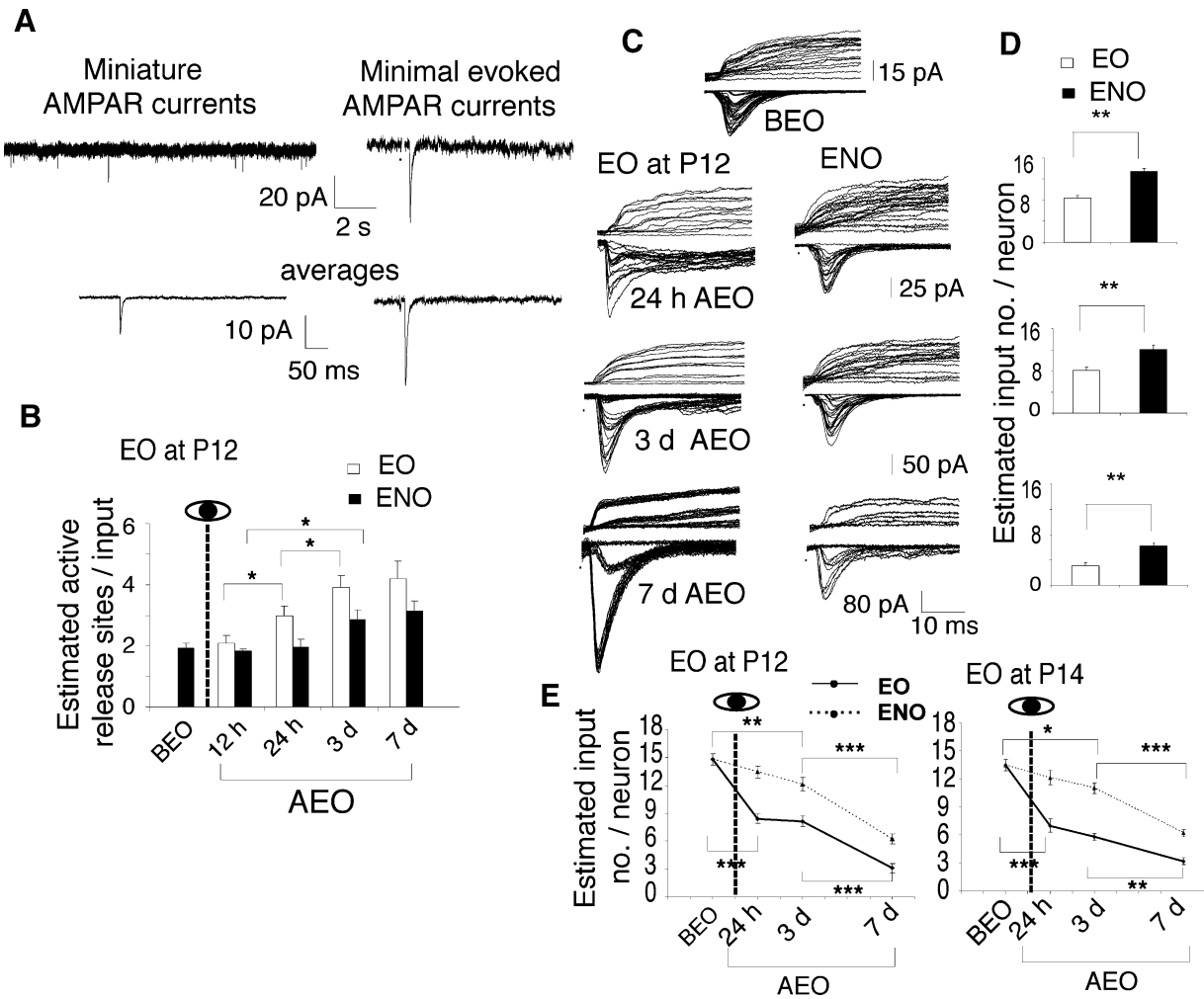
Figure 7. Number of Release Sites per Input Increases, and the Number of Inputs per Neuron Decreases Rapidly AEO

(A) An average mAMPARc (left) and an average minimal evoked AMPAR current (right) from the same neuron as well as samples of the recordings from which these averages were taken. The ratio of average amplitude of the minimal evoked AMPAR current over the average amplitude of the mAMPARc was used as an estimator of the number of active vesicle release sites between the presumably single axons that were stimulated and the postsynaptic neuron that was examined in voltage clamp. This is a measure of relative change, but it is probably a large underestimate of the actual number of changing inputs (see text).

(B) Significant increases in numbers of release sites occur within 24 hr AEO, indicating that increased consolidation of some inputs occurs rapidly and continues to increase at 3 days AEO. ENO pups also show an increase, but this is only seen at 3 days AEO. At least 6 and up to 8 neurons were studied for each data point.

(C) The number of inputs per postsynaptic neuron estimated BEO and AEO using the method of shoulders indicates that synapse elimination occurred rapidly and then continued with a slower decline for at least a week AEO. NMDAR currents shown in the figure are those taken in the presence of NBQX after the initial determination of AMPAR/KAR and AMPAR/KAR plus NMDAR currents. KARs were not selectively blocked in these experiments. Stimuli were delivered at the rostral end of the stratum opticum, where afferent axons are dense.

(D) Quantitative comparisons in input number between EO and ENO littermates. n = at least 6 and up to 9 neurons for each bar graph.

(E) Plots of changes in input number per neuron BEO and at three time points AEO. n = at least 6 and at most 9 neurons for each data point.

With the onset of high-contrast pattern vision, there is a pronounced change in the amount and temporal patterning of activity that is transmitted by the retina, and the visual cortex is particularly responsive to such input (Rodieck, 1998). Around EO, the corticocollicular projection begins to arborize profusely (Thong and Dreher, 1986; Colonnese and Constantine-Paton, 2001) and begins to influence sSC neuron receptive fields (Binns and Salt, 1997). It is tempting to speculate that the synaptic changes that were detected in this study reflect the active sprouting of the cortical inputs.

Visual Synapse Change after the Onset of Pattern Vision

Many investigators have used dark rearing with an introduction to light to control the onset of vision. Quinlan et al. (1999a, 1999b) applied this paradigm to show that currents apparently mediated by NR2A-rich NMDARs rapidly appear at visual cortical synapses 2 hr after the first visual experience, and Binns and Salt (1998) reported greater NMDAR contributions to visually driven activity in dark-reared versus normally reared rats. However, controlled EO and dark rearing with light exposure

are not the same treatment. Diffuse stimulation through closed lids drives some maturational changes at visual synapses (Shi et al., 2000; Akerman et al., 2002; Townsend et al., 2003), implying that synapses in animals that are maintained in darkness are different from those in animals in which low levels of ambient light or diffuse patterns stimulate the retina.

Several studies have described changes in visual system synaptic currents occurring after natural EO. Desai et al. (2002), recording from visual cortex, found an increase in the frequency of miniature AMPAR currents and, in contrast to the work presented here, a decrease in miniature AMPAR current amplitude after EO. This was not observed in dark-reared animals. However, the event reported by Desai et al. (2002) occurred ~3–4 days AEO. At roughly this latency, after controlled EO in the sSC, our recordings revealed an increase in what we find to be kainate receptor (KAR) currents that then decreased over the next 2 weeks. The KAR contribution makes the non-NMDAR glutamate current in the sSC appear to grow in amplitude (see Figure 7C; 7 days AEO). The true AMPAR current does not significantly change in amplitude throughout the 2 week post-EO interval (Figure 5C; W.L. and M.C.-P., unpublished data). KAR currents are not distinguished from AMPAR currents by many antagonists, and this may be the cause of the discrepancy between the cortical work and our own. Alternatively, non-NMDAR ionotropic glutamate receptors may respond differently to EO in different visual regions. Chen and Regehr (2000) also reported post-EO changes in the visual synapses of the dorsal-lateral geniculate nucleus that are fully consistent with this report. However, they did not control EO and explore the sequence of events within the first 24 hr AEO.

The Yoshii et al. (2003) study that found that levels of PSD-95 increased ~300% in visual neuron dendrites within 6 hr AEO motivated the present functional study. While the current data cannot prove that PSD-95 movement to visual dendrites with EO is the only mechanism mediating the changes that we describe in this report, the nature and the timing of these changes are consistent with the hypothesis that EO-induced PSD-95 movement to visual synapses is the mechanism responsible for initiating these events.

PSD-95 Biology Relevant to Receptor Trafficking
The membrane-associated guanylate kinases (MAGUKs) are clustering proteins that are implicated in the positioning of transmembrane molecules. PSD-95 and SAP 102 are the MAGUKs that are associated with ionotropic glutamate receptor scaffolding in the visual cortex and the sSC (Yoshii et al., 2003; Van Zundert et al., 2004). PSD-95 is a major postsynaptic density (PSD) molecule (Cho et al., 1992) and clusters NMDARs at the synapse (Niethammer et al., 1996). In addition to the NMDARs, many molecules associated with receptor signaling are held at the postsynaptic membrane by the PDZ or SH3 domains of PSD-95 (Kennedy, 2000; Sheng, 2001; Komiyama et al., 2002). Thus, PSD-95 is a major organizer of the mature NMDAR effector complex. However, PDZ domains of PSD-95 can also bind the stargazin family of transmembrane AMPAR regulatory proteins (TARPS; Tomita et al., 2003), and through its stargazin interaction,

PSD-95 has also been implicated in clustering and stabilizing AMPARs at the synapse (Chen et al., 2000; Schnell et al., 2002; Tomita et al., 2003). Furthermore, within 6 hr of controlled EO both PSD-95/stargazin complexes as well as the PSD-95/NR2A-rich NMDAR complexes are enriched in dendrites of visual cortical and sSC neurons (Yoshii et al., 2003). Therefore, it is not surprising that both NMDAR and AMPAR synaptic currents show rapid changes AEO. The issue is how many of these changes are directly tied to the subsynaptic insertion of newly arrived PSD-95.

Recent transfection experiments support the idea that PSD-95 increases at visual synapses initiate most of these changes. PSD-95-GFP overexpressed in neocortical (Beique and Andrade, 2003; Ehrlich and Malinow, 2004) or hippocampal neurons (Stein et al., 2003) results in transfected neurons having more AMPAR miniature events (Beique and Andrade, 2003; Stein et al., 2003; Ehrlich and Malinow, 2004) and also expressing more functional AMPARs at each contact (Stein et al., 2003; Ehrlich and Malinow, 2004) compared with neighboring neurons that express only endogenous amounts of PSD-95. Also, LTP is occluded, and long-term depression (LTD) is increased in cortical and hippocampal neurons overexpressing PSD-95 (Stein et al., 2003; Ehrlich and Malinow, 2004) but not in untransfected neighbors. These data indicate that high levels of cytoplasmic PSD-95 enable neurons to insert more AMPAR currents into their synapses. In contrast, overexpression of PSD-95 in cerebellar granule cells increases the ratio of the NR2A to NR2B subunit when NMDAR miniature currents are examined (Losi et al., 2003). Together, these data indicate that synaptic changes in both NMDAR and AMPAR currents can be initiated by increasing PSD-95 at the postsynaptic membrane.

There is accumulating evidence that, in vivo, NR2A-rich and NR2B-rich NMDARs are held at synapses by PSD-95 and SAP-102, respectively. Only receptors with both NR2A and NR2B appear to be held by both MAGUKs (Van Zundert et al., 2004). PSD-95 holds NMDARs by the NR2A C terminus and is unable to effectively bind endogenous NMDARs when only the NR2B C terminus is present (Steigerwald et al., 2000; Townsend et al., 2003). SAP 102 predominates in the late fetal and early postnatal brain and coexists at lower levels with PSD-95 at some mature synapses (Sans et al., 2000). SAP-102 appears to be constitutively present at glutamate synapses, and endogenous SAP-102 is associated with higher proportions of NR2B than PSD-95 (Sans et al., 2000; Yoshii et al., 2003). Also, in maturing neurons SAP-102 and NR2B-rich NMDARs are most frequently present in extra- and perisynaptic regions, while PSD-95 is associated mostly with the PSD (Tovar and Westbrook, 1999; Sans et al., 2000). In the sSC, before EO NR2A-mediated currents gradually become more prevalent in miniature NMDARs, while evoked NMDAR currents, involving extrasynaptic receptors, retain currents with larger contributions from NR2B-rich NMDARs (Van Zundert et al., 2004).

The EO period in the sSC is associated with a decrease, not an increase, in transcript and protein for the NR2B subunit (Shi et al., 1997). Consequently, the SS currents that are carried by NR2B-rich receptors observed here must be mediated by extrasynaptic
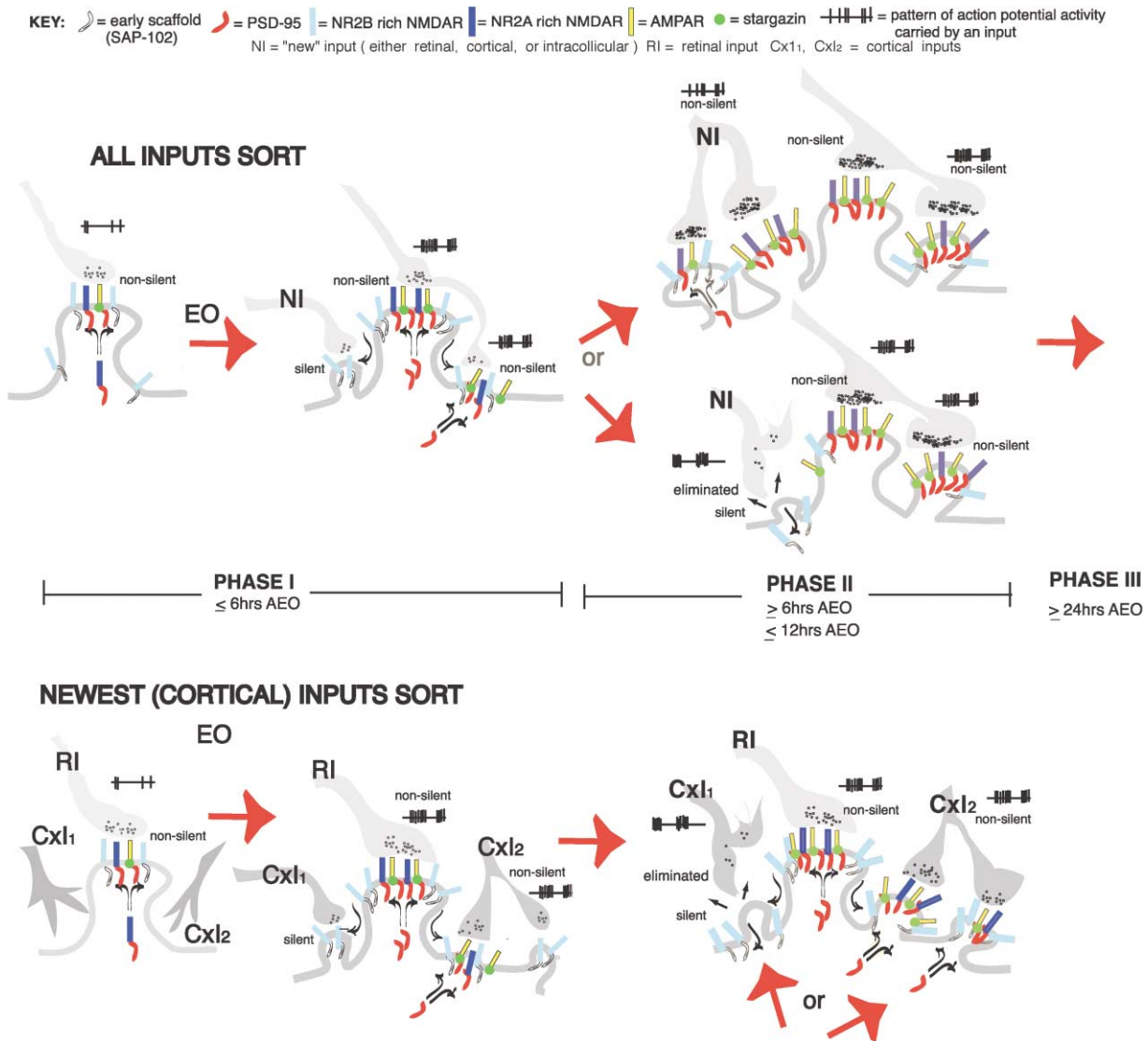
Figure 8. A Model of Activity-Dependent Receptor Trafficking, Synaptogenesis, and Refinement in the First 24 Hr AEO

The three phases of synaptic NMDAR and AMPAR current change are identified as a function of EO-induced, activity-dependent PSD-95 transport to and insertion at synapses. The model depicts but does not require the association between NR2B-rich receptors and the MAGUK SAP-102. The key element of the model is that NR2B-only extrasynaptic receptors are the mediators of signaling at the initial contacts between post- and presynaptic elements. These are "silent" synapses. Nascent contacts onto postsynaptic surfaces with sufficient depolarization to drive the "extrasynaptic" NMDARs are reinforced by PSD-95 that can then stabilize AMPARs and enrich for NR2A NMDARs at the increasingly stable contacts. The current data do not discriminate between retinal synapses, intracollicular synapses, and cortical synapses. Therefore, the two extremes of the possible dynamics are diagrammed. In the upper sequence, all synapses in the sSC are presumed to be labile and to compete for collicular neuron dendritic sites on the basis of new temporal patterns of activity in the retinal and cortical projections resulting from the onset of pattern vision. In the lower sequence, the corticocollicular projection, which begins to arborize in the sSC around the time of EO, is the major source of shifting synapses. The retinal inputs are assumed to be stable by this stage. Consequently, the cortical inputs, which are driven effectively during patterned visual stimulation, sort in order to establish the corticocollicular map in register with the retinocollicular map. The phases of the model are discussed in more detail in the text.

NMDARs using preexisting NR2B subunits or entire NR2B/SAP-102 receptor scaffolding complexes.

A Model of Activity-Mediated Synaptogenesis and Refinement In Vivo
Figure 8 diagrams the present post-EO observations as a direct consequence of activity-dependent targeting of PSD-95 to visual synapses. Two extreme versions of the model are illustrated. The upper version is the more general of the two, in which any or all of the inputs to the sSC—retinal, intracollicular, or cortical—can be altered by the changed temporal patterning of activity. The lower version assumes that only cortical inputs sort in order to produce registration between retinal and cortical representations of visual space.

There are three distinct phases to this late wave of synaptogenesis. During phase I, heightened afferent activity increases PSD-95 in visual dendrites and then

PSD-95 insertion at the center of the PSD. This insertion displaces preexisting NR2B-rich NMDARs to extrasynaptic membrane (Townsend et al., 2003) where NR2B-rich receptors have been localized in cultured neurons (Tovar and Westbrook, 1999). These extrasynaptic NR2B-rich receptors have a high probability of being contacted by glutamate-releasing terminals as a result of an activity-induced increased motility of the dendritic membrane (Sin et al., 2002; Niell et al., 2004). Thus, new, NR2B "only" NMDAR contacts are formed and detected as SS NMDAR currents. This event also produces the transient increase in silent synapses, because many have not yet added AMPARs to their active sites. During phase II, the continued presence of SS NMDAR currents and possibly the buildup of displaced NR2B-rich NMDARs produce the transient increase in NMDAR evoked currents (Figure 3). At the same time, however, PSD-95 begins to hold both NR2A-rich NMDARs and stargazin-AMPAR channel complexes at the PSD, and FB sNMDAR currents show faster decay times (Figure 1C), while miniature AMPAR currents show an increase in amplitude (Figure 5C). In addition, many of the silent synapses with correlated activity add AMPAR currents through stargazin binding to PSD-95, and this addition results in the significant increase in miniature AMPAR current frequency (Figure 5C).

Finally, during phase III, beginning ~24 hr AEO, different PSD-95 molecules have bound NR2A-rich receptors and AMPARs at the new and surviving synapses of sSC neurons (Figure 5). Continued pattern-driven activity maintains increases in AMPAR currents, begins to decrease NMDAR current amplitude at mature synapses (detected as amplitude decreases in FB NMDAR spontaneous currents; Figure 1C), and probably consolidates inputs from many axons to fewer axons, each with more contacts impinging on each cell (Figure 7). Consequently, the potentiation of the AMPAR currents that was detected in miniature currents at 12 hr becomes detectable as an increase in the AMPAR:NMDAR evoked current ratio (Figure 6B). The continued increase in the frequency of SS NMDAR currents, despite a decrease in silent synapses at this time, probably reflects that new synapses are being formed and then either reinforced with AMPARs or dissolved as the maturation of sSC circuitry continues (Figure 7). By 1 week AEO, the SS currents have completely disappeared from the neuropil, an event that may initiate the close of EO-induced synaptic refinement at sSC glutamate synapses. Phase III is therefore prolonged and is not diagrammed in Figure 8.

Conclusions

This model accounts for current findings and is consistent with much earlier work. It does not attempt to incorporate the numerous additional interactions that are involved in synaptogenesis or plasticity, but it may suggest points in the synaptogenetic process where many of these interactions are employed. Irrespective of the model, however, the data in this report show that the first functional synaptic changes that are induced by EO are in NMDARs and silent synapses. Increases in miniature AMPAR current frequency and amplitude indicative of LTP are only detected after the first NMDAR

changes (12 hr AEO). Not until 24 hr AEO are larger AMPAR:NMDAR evoked current ratios observed. This study also demonstrates that normal developmental increases in sensory activity in vivo rapidly drive cellular and molecular mechanisms of synaptic potentiation. We postulate that these in vivo changes utilize exactly the same mechanisms that mediate NMDAR-dependent LTP. Most significantly, however, at the single neuron level, these EO-induced changes in currents are coincident with and probably responsible for the input reinforcement and elimination that refines central nervous system local circuits for optimal function in the sensory world.

Experimental Procedures

Animal Treatment

Pregnant Sprague-Dawley female rats were purchased and allowed to give birth at MIT. The day of birth (P0) was accurately ascertained. P10 pups were anesthetized with brief exposure to ether, and both eyelids were sealed with Vetbond (3M) tissue glue. Mothers with their litters were then maintained in constant ambient light to allow time for visual experience, slice preparation, and recording of both EO and control littermates (see following) on the same day without a shortly preceding exposure to a dark cycle. EO (removing the glue and opening the eyelids) was accomplished on half the pups in each litter after isofluorane anesthesia. ENO pups were examined daily, and more glue was added when it was deemed necessary to avoid spontaneous EO. Animals that achieved spontaneous EO were not used. Pups remained with their mother, while pairs (one EO and one ENO) were removed at fixed intervals for sacrifice and physiological analyses. Midbrain slices from each pair of pups were examined at intervals of 6 hr, 12 hr, 24 hr, 3 days, and 7 days AEO. Consequently, comparisons between pups with EO and with ENO at each interval were made with roughly equal numbers of pups from each litter. For the preparation of brain slices, pups were anesthetized with ether and decapitated prior to dissection of the midbrain. All procedures followed MIT IACUC-approved protocols.

Electrophysiology

Recordings were from neurons of the stratum griseum superficiale of the superior colliculus in 350 μm parasaggital sections of the midbrain. Recorded neurons were imaged with infrared differential interference contrast and ranged in soma size from 15 to 20 μM. This size range and location enriched for narrow field vertical neurons but probably also included some piriform cells (Langer and Lund, 1974). Vibratome slices were equilibrated in ACSF (117 mM NaCl, 4 mM MgCl$_2$, 4 mM KCl, 1.2 mM NaHPO$_4$, 26 mM NaHCO$_3$, 4 mM CaCl$_2$ × 2H$_2$O, 15 mM glucose, and 2 μM glycine) for at least 1 hr prior to recording. Recording pipettes (5–10 mΩ) were filled with 122.5 mM Cs-gluconate, 17.5 mM CsCl, 8 mM CaCl2, 10 mM HEPES (CsOH), 0.2 mM Na-EGTA, 2 mM Mg-ATP, and 0.3 mM Na-GTP at pH 7.2–7.4. All neurons maintained seal resistances of above 5 GΩ. Series resistances were <40 MΩ, and input resistances were 800–900 MΩ. Electrical stimuli used bipolar electrodes composed of a pair of tungsten microelectrodes (WPI) with tip separation of ~250 μm. Recordings used an Axopatch 220B amplifier, a Digidata 1322A interface, and a PC running Axoclamp software. Currents were sampled at 10 kHz and filtered at 5 kHZ. Evoked AMPAR:NMDAR current ratios were recorded using stimulus intensities midway between threshold and saturation. For evoked AMPAR current recording, BMI (10 μm), D,L-AP5 (50 μm), and SIM2081 (10–50 μm) were added to the ACSF while holding the voltage at −70 mV. Recordings were made ~3 min after the onset of perfusing with SIM2081 added. SIM2081 is a highly specific kainate receptor (KAR) agonist that rapidly desensitizes KARs and eliminates KAR currents from recordings (Savidge et al., 1999; Cossart et al., 2002). In general, evoked NMDAR current recordings were made at +40 mV with BMI (10 μm) and NBQX (10 μm) in the ACSF. Spontaneous NMDAR current recordings were made at −70 mV with the same antagonists but with Mg^{2+} removed from the ACSF. AMPAR miniature currents were recorded at −70

mV with BMI (10 μm), D,L-AP5 (50 μm), SIM2081 (50 μm) and TTX (1 μm) in the bath. The NR2B-mediated component of NMDAR currents was assayed in pharmacologically isolated currents in cells held at −70 mV in 0 mM Mg^{2+} and 3 μM ifenprodil. Minimal stimulation was achieved by gradually increasing stimulating current from zero until the first evoked currents were observed (2–6 μA). Repetition of this stimulus with either a failure or the same evoked current was considered activation of a single axon. Estimations of the number of inputs converging on a single sSC neuron used gradually increasing stimulating currents. Criteria for distinguishing an increase in the evoked current as a contribution for an additional axon were a clear-cut shoulder on the evoked current rising phase and the stability of this response to multiple stimuli of the same intensity.

Silent Synapse Protocol
A minimal stimulus was applied at intervals of at least 1 min, while the holding voltage was switched between −70 mV and +40 mV. With stimulating intensity held constant, a reproducible evoked outward current at +40 mV with no evoked AMPA current detectable at −70 mV was a potential silent synapse. Criterion for "silent" was at least six to ten consecutive trials alternating between −70 and +40 mV showing an outward current at +40 mV without an inward current at −70 mV. To control for variability between litters, at least three litters were used for each time point. The average and standard deviation for each point was then calculated from all three litters, where the contribution from each litter was the total number of neurons with silent synapses in the litter over the total number of neurons recorded in that litter. Statistics compared the mean and standard deviations of the litter averages for each time point that was examined. Data for evoked NMDAR currents at +40 mV isolated by the addition of NBQX (pictured in Figures 4A and 4B) were obtained after the tests for silent versus nonsilent inputs on each neuron were complete.

Data Analysis
Synaptic currents were characterized by the following parameters: peak amplitude, rise time (10%–90% of peak amplitude). Decay time was fitted from 100%–0% peak amplitude with a single exponential and is given in ms throughout the text as decay interval measured at 0.37 peak amplitude. The average for each value was obtained using Minianalysis 5.1. Baseline noise ranged from 2.5–5.0 pA peak to peak, and synaptic events with an amplitude 2 times 1/2 peak-to-peak noise were analyzed. Spontaneous events were measured in a total of 75 s of recording from each neuron chosen randomly throughout the recording period.

Drugs
D,L-AP5, BMI, cyclothiazide (CTZ), and TTX were from Sigma. NBQX, ifenprodil, and SYM 2081 were from Tocris.

Statistical Analyses
A two-tailed ANOVA followed by the Tukey post hoc test was used to detect intervals in which significant changes occurred for all data sets where a parameter was measured across time points within a treatment. Student's t tests were applied when two populations of responses were examined. A nonparametric paired sample Sign test was applied when responses in age-matched EO versus ENO littermates were compared. A parametric test could not be used in such two-sample comparisons, because the variation in measurements at each time point for the ENO animals was always less than that for their AEO littermates. In all figures, error bars represent the SEM; *$p \leq 0.05$, **$p \leq 0.01$, ***$p \leq 0.001$.

References

Akerman, C.J., Smyth, D., and Thompson, I.D. (2002). Visual experience before eye-opening and the development of the retinogeniculate pathway. Neuron *36*, 869–879.

Bansal, A., Singer, J.H., Hwang, B.J., Xu, W., Beaudet, A., and Feller, M.B. (2000). Mice lacking specific nicotinic acetylcholine receptor subunits exhibit dramatically altered spontaneous activity patterns and reveal a limited role for retinal waves in forming ON and OFF circuits in the inner retina. J. Neurosci. *20*, 7672–7681.

Bear, M.F., Kleinschmidt, A., Gu, Q.A., and Singer, W. (1990). Disruption of experience-dependent synaptic modifications in striate cortex by infusion of an NMDA receptor antagonist. J. Neurosci. *10*, 909–924.

Beique, J.C., and Andrade, R. (2003). PSD-95 regulates synaptic transmission and plasticity in rat cerebral cortex. J. Physiol. *546*, 859–867.

Binns, K.E., and Salt, T.E. (1997). Post eye-opening maturation of visual receptive field diameters in the superior colliculus of normal- and dark-reared rats. Brain Res. Dev. Brain Res. *99*, 263–266.

Binns, K.E., and Salt, T.E. (1998). Developmental changes in NMDA receptor-mediated visual activity in the rat superior colliculus, and the effect of dark rearing. Exp. Brain Res. *120*, 335–344.

Bolshakov, V.Y., Golan, H., Kandel, E.R., and Siegelbaum, S.A. (1997). Recruitment of new sites of synaptic transmission during the cAMP-dependent late phase of LTP at CA3-CA1 synapses in the hippocampus. Neuron *19*, 635–651.

Chen, C., and Regehr, W.J. (2000). Developmental remodeling of the retinogeniculate synapse. Neuron *28*, 955–966.

Chen, L., Chetkovich, D.M., Petralia, R.S., Sweeney, N.T., Kawasaki, Y., Wenthold, R.J., Bredt, D.S., and Nicoll, R.A. (2000). Stargazing regulates synaptic targeting of AMPA receptors by two distinct mechanisms. Nature *408*, 936–943.

Cho, K.O., Hunt, C.A., and Kennedy, M.B. (1992). The rat brain postsynaptic density fraction contains a homolog of the *Drosophila* discs-large tumor suppressor protein. Neuron *9*, 929–942.

Cline, H.T., Debski, E., and Constantine-Paton, M. (1987). NMDA receptor antagonist desegregates eye-specific stripes. Proc. Natl. Acad. Sci. USA *84*, 4342–4345.

Colonnese, M.T., and Constantine-Paton, M. (2001). Chronic NMDA receptor blockade from birth increases the sprouting capacity of ipsilateral retinocollicular axons without disrupting their early segregation. J. Neurosci. *21*, 1557–1568.

Constantine-Paton, M., and Cline, H.T. (1998). LTP and activity-dependent synaptogenesis: the more alike they are, the more different they become. Curr. Opin. Neurobiol. *8*, 139–148.

Cossart, R., Epsztein, J., Tyzio, R., Becq, H., Hirsch, J., Ben-Ari, Y., and Crepel, V. (2002). Quantal release of glutamate generates pure kainate and mixed AMPA/kainate EPSCs in hippocampal neurons. Neuron *35*, 147–159.

Desai, N.S., Cudmore, R.H., Nelson, S.B., and Turrigiano, G.G. (2002). Critical periods for experience-dependent synaptic scaling in visual cortex. Nat. Neurosci. *5*, 783–789.

Drager, U.C., and Hubel, D.H. (1976). Topography of visual and somatosensory projections to mouse superior colliculus. J. Neurophysiol. *39*, 91–101.

Durand, G.M., Kovalchuk, Y., and Konnerth, A. (1996). Long-term potentiation and functional synapse induction in developing hippocampus. Nature *381*, 71–75.

Ehrlich, I.D., and Malinow, R. (2004). Postsynaptic density 95 controls AMPA receptor incorporation during long-term potentiation and experience-driven synaptic plasticity. J. Neurosci. *24*, 916–927.

Flint, A.C., Maisch, U.S., Weishaupt, J.H., Kreigstein, A.R., and Monyer, H. (1997). NR2A subunit expression shortens NMDA synaptic currents in developing neocortex. J. Neurosci. *17*, 2469–2476.

Fox, K., Daw, N., Sato, H., and Czepita, D. (1991). Dark-rearing delays the loss of NMDA receptor function in the kitten visual cortex. Nature *350*, 342–344.

Hohnke, C.D., Oray, S., and Sur, M. (2000). Activity-dependent pat-

terning of retinogeniculate axons proceeds with a constant contribu-
tion from AMPA and NMDA receptors. J. Neurosci. 20, 8051–8060.

Isaac, J.T.R., Crair, M.C., Nicoll, R.A., and Malenka, R.C. (1997).
Silent synapse during development of thalamocortical inputs. Neu-
ron 18, 269–280.

Kennedy, M.B. (2000). Signal-processing machines at the postsyn-
aptic density. Science 290, 750–754.

Komiyama, N.H., Watabe, A.M., Carlisle, H.J., Porter, K.,
Charlesworth, P., Monti, J., Strathdee, D.J.C., O'Carroll, C.M., Mar-
tin, S.J., Morris, R.G., et al. (2002). SynGAP regulates ERK/MAPK
signaling, synaptic plasticity, and learning in the complex with post-
synaptic density 95 and NMDA receptor. J. Neurosci. 22, 9721–9732.

Langer, T.P., and Lund, R.D. (1974). The upper layers of the superior
colliculus of the rat: a Golgi study. J. Comp. Neurol. 158, 418–435.

Li, Y., Erzurumlu, R.S., Chen, C., Jhaveri, S., and Tonegawa, S.
(1994). Whisker-related neuronal patterns fail to develop in the tri-
geminal brain stem nuclei of NMDAR1 knockout mice. Cell 76,
427–437.

Linden, R., and Perry, V.H. (1983). Massive retinotectal projection
in rats. Brain Res. 272, 145–149.

Losi, G., Prybylowski, K., Fu, Z., Luo, J., Wenthold, R.J., and Vicini, S.
(2003). PSD-95 regulates NMDA receptors in developing cerebellar
granule neurons of the rat. J. Physiol. 548, 21–29.

Lund, R.D. (1972). Anatomic studies on the superior colliculus. In-
vest. Ophthalmol. 11, 434–441.

Malinow, R., and Malenka, R.C. (2002). AMPA receptor trafficking
and synapse plasticity. Annu. Rev. Neurosci. 25, 103–126.

Monyer, H., Burnashev, N., Laurie, D.J., Sakmann, B., and Seeburg,
P.H. (1994). Developmental and regional expression in the rat brain
and functional properties of four NMDA receptors. Neuron 12,
529–540.

Niell, C.M., Meyer, M.P., and Smith, S.J. (2004). In vivo imaging
of synapse formation on a growing dendritic arbor. Nat. Neurosci.
7, 254–260.

Niethammer, M., Kim, E., and Sheng, M. (1996). Interaction between
the C terminus of NMDA receptor subunits and multiple members
of the PSD-95 family of membrane-associated guanylate kinases.
J. Neurosci. 16, 2157–2163.

Oliet, S.H., Malenka, R.C., and Nicoll, R.A. (1996). Bidirectonal con-
trol of quantal size by synaptic activity in the hippocampus. Science
271, 1294–1297.

Purves, D., and Lichtman, J.W. (1985). Principles of Neural Develop-
ment (Sunderland, MA: Sinaur Associates).

Quinlan, E.M., Philpot, B.D., Huganir, R.L., and Bear, M.F. (1999a).
Rapid, experience-dependent expression of synaptic NMDA recep-
tors in visual cortex in vivo. Nat. Neurosci. 2, 352–357.

Quinlan, E.M., Olstein, D.H., and Bear, M.F. (1999b). Bidirectional,
experience-dependent regulation of N-methyl-D-aspartate receptor
subunit composition in the rat visual cortex during postnatal devel-
opment. Proc. Natl. Acad. Sci. USA 96, 12876–12880.

Rodieck, R.W. (1998). The First Steps in Seeing (Sunderland, MA:
Sinauer Assoc. Inc.).

Sans, N., Petralia, R.S., Wang, Y.-X., Blahos, J., II, Hell, J.W., and
Wenthold, R.J. (2000). A developmental change in NMDA receptor-
associated proteins at hippocampal synapses. J. Neurosci. 20,
1260–1271.

Savidge, J.R., Sturgess, N.C., Bristow, D.R., and Lock, E.A. (1999).
Characterization of kainate receptor mediated whole-cell currents
in rat cultured cerebellar granule cells. Neuropharmacology. 38,
375–382.

Schnell, E., Sizemore, M., Karimzadegan, S., Chen, L., Bredt, D.S.,
and Nicoll, R.A. (2002). Direct interactions between PSD-95 and
stargazin control synaptic AMPA receptor number. Proc. Natl. Acad.
Sci. USA 99, 13902–13907.

Sheng, M. (2001). Molecular organization of the postsynaptic spe-
cialization. Proc. Natl. Acad. Sci. USA 13, 7058–7061.

Shi, J., Aamodt, S.M., and Constantine-Paton, M. (1997). Temporal
correlations between functional and molecular changes in NMDA

receptors and GABA neurotransmission in the superior colliculus.
J. Neurosci. 17, 6264–6276.

Shi, J., Townsend, M., and Constantine-Paton, M. (2000). Activity-
dependent induction of tonic calcineurin activity mediates a rapid
developmental downregulation of NMDA receptor currents. Neuron
28, 103–114.

Simon, D., and O'Leary, D. (1992). Development of topographic order
in the mammalian retinocollicular projection. J. Neurosci. 12, 1212–
1232.

Simon, D.K., Prusky, G.T., O'Leary, D.D.M., and Constantine-Paton,
M. (1992). NMDA receptor blockade interferes with development of
neural maps in the mammalian brain. Proc. Natl. Acad. Sci. USA
89, 10593–10597.

Sin, W.C., Haas, K., Ruthazer, E.S., and Cline, H.T. (2002). Dendrite
growth increased by visual activity requires NMDA receptor and
Rho GTPases. Nature 419, 475–480.

Singer, W. (1995). Development and plasticity of cortical processing
architectures. Science 270, 758–764.

Steigerwald, F., Schultz, T.W., Schenker, L.T., Kennedy, M.B., See-
burg, P.H., and Kohr, G. (2000). C-terminal truncation of NR2A sub-
units impairs synaptic but not extrasynaptic localization of NMDARs.
J. Neurosci. 20, 4573–4581.

Stein, V., House, D.R.C., Bredt, D.S., and Nicoll, R.S. (2003). Postsyn-
aptic density-95 mimics and occludes hippocampal long-term po-
tentiation and enhances long-term depression. J. Neurosci. 23,
5503–5506.

Thong, I.G., and Dreher, B. (1986). The development of the cortico-
tectal pathway in the albino rat. Brain Res. 390, 227–238.

Tomita, S., Chen, L., Kawasaki, Y., Petralia, R.S., Wenthold, R.J.,
Nicoll, R.A., and Bredt, D.S. (2003). Functional studies and distribu-
tion define a family of transmembrane AMPA receptor regulatory
proteins. J. Cell Biol. 161, 805–861.

Toni, N., Buchs, P.A., Nikonenko, I., Bron, C.R., and Muller, D. (1999).
LTP promotes formation of multiple spine synapses between a sin-
gle axon terminal and a dendrite. Nature 402, 421–425.

Tovar, K.R., and Westbrook, G.L. (1999). The incorporation of NMDA
receptors with a distinct subunit composition at nascent hippocam-
pal synapses in vitro. J. Neurosci. 19, 4180–4188.

Townsend, M., Yoshii, A., Mishina, M., and Constantine-Paton, M.
(2003). Developmental loss of miniature N-methyl-D-asparate recep-
tor currents in NR2A knockout mice. Proc. Natl. Acad. Sci. USA
89, 10593–10597.

Van Zundert, B., Yoshii, A., and Constantine-Paton, M. (2004). Re-
ceptor compartmentalization and trafficking at glutamate synapses:
A developmental proposal. Trends Neurosci., in press.

Williams, K., Russel, S.L., Shen, Y.M., and Molinoff, P.B. (1993).
Developmental switch in the expression of NMDA receptors occurs
in vivo and in vitro. Neuron 10, 267–278.

Wu, G.-Y., Malinow, R., and Cline, H.T. (1996). Maturation of a central
glutamatergic synapse. Science 274, 972–976.

Yoshii, A., Sheng, M.H., and Constantine-Paton, M. (2003). Eye
opening induces a rapid dendritic localization of PSD-95 in central
visual neurons. Proc. Natl. Acad. Sci. USA 100, 1334–1339.

Zhang, L.L., Tao, H.W., and Poo, M. (2000). Visual input induces
long-term potentiation of developing retinotectal synapses. Nat.
Neurosci. 3, 708–718.